PAPER

Check for updates

Facile formulation of a long-wavelength cyanine for optical imaging in the second near-infrared window†

Hailey I. Kilian,[a] Homan Kang, [b] Nikhila Nyayapathi,[a] Takeshi Fukuda,[b] Eeswar Adluru,[b] Huijuan Zhang,[a] Breandan Quinn,[a] Jun Xia,[a] Hak Soo Choi [b] and Jonathan F. Lovell [b] *[a]

The second near-infrared window (NIR-II) beyond 1000 nm has attracted attention for optical contrast imaging in small animals. We sought to assess whether commercially available NIR-II dyes could be easily formulated for this purpose. 13 hydrophobic NIR-II dyes were purchased and screened by formulating them in simple solubilizing agents with established use in humans: propylene glycol, Cremaphor EL, Kolliphor HS15 (HS15), Tween 80, and cyclodextrin. Based on the absorption at 1064 nm (matching the Nd:YAG laser output commonly used in photoacoustic imaging), three of the dyes were further assessed at varying dye and surfactant concentrations. Of these, benzo indole butyl diphenylaminocyclopentene heptamethine (BIBDAH) tetrafluoroborate in HS15 generally showed the most favorable NIR-II character. 1 mg mL^{-1} BIBDAH in 25% HS15 exhibited a single absorption peak at 1030 nm with a calculated intensity greater than 100, which was relatively stable for weeks in storage. Following intravenous administration to mice, determination of BIBDAH pharmacokinetics was possible by absorption measurements of sampled plasma, revealing a circulating half-life of about one hour. Most of the dye was taken up by the liver. BIBDAH was used *in vitro* and *in vivo* as a photoacoustic contrast imaging agent and its accumulation could be detected in subcutaneous tumors in mice. BIBDAH was used for fluorescence imaging of blood vessels in mice, including in the brain (through intact skull), and dye clearance from blood to the liver was visualized. Taken together, this study confirms that accessible, strongly-absorbing dye can readily be formulated for injection by simply dissolving them in biocompatible surfactants and used for high-contrast preclinical optical imaging in the second NIR window.

[a]*Department of Biomedical Engineering, University at Buffalo, State University of New York, Buffalo, NY 14260, USA. E-mail: jflovell@buffalo.edu*
[b]*Gordon Center for Medical Imaging, Department of Radiology, Massachusetts General Hospital and Harvard Medical School, Boston, MA 02114, USA*
†Electronic supplementary information (ESI) available. See DOI: 10.1039/d0bm00572j

Introduction

The near-infrared (NIR) spectral region is used for preclinical and clinical optical imaging, as tissue interference is lower compared to the visible region.[1] Indocyanine green and methylene blue are the only two clinically-used NIR dyes, with absorption maxima around 800 and 670 nm respectively.[2] Despite the utility of fluorescence contrast imaging, it is limited by shallow depth penetration due primarily to light scattering in tissues. Longer wavelength optical imaging, in the so-called second NIR window (NIR-II) in the range of 1000–1700 nm has inherently diminished tissue scattering, and holds promise for biomedical imaging. Photoacoustic imaging (PAI) also addresses light scattering by using ultrasound-based detection, a signal which is resistant to tissue scattering.[3] In particular, PAI contrast agents that absorb light at the specific NIR-II wavelength of 1064 nm are useful as they match output of the ND:YAG laser used in PAI, and the permissible laser power for humans is higher compared to visible range wavelengths.

NIR-II contrast agents have been developed for fluorescence and photoacoustic imaging. These include nanoparticles based on quantum dots,[4–9] semi-conducting polymers,[10–12] lanthanide-doping,[13] and gold.[14–16] Small molecule dyes have also been synthesized for NIR-II imaging based on structures like benzo-bis(1,2,5-thiadiazole),[17,18] cyanine,[19,20] phthalocyanine,[21] and others.[22] Activatable NIR-II molecular probes have been developed.[23] Without chemical functionalization, NIR-II dyes tend to be hydrophobic, and thus require a solubilization approach for intravenous administration. Albumin has been used as a carrier for NIR-II dyes.[24,25] Our lab developed

an approach of surfactant-stripping of organic NIR dyes,[26] which resulted in concentrated formulations of an NIR-II dye for PAI.[27]

Despite progress in the development of NIR-II nanoparticles and dyes, simple-to-prepare high-contrast agents are not readily available at present, to the best of our knowledge. A biocompatible contrast agent that could be prepared as readily as methylene blue (*i.e.* by simply dissolving powdered dye in an aqueous medium) could be useful for use in general imaging studies. In this study we aim to address this by screening commercially available hydrophobic NIR-II dyes for suitability to be prepared by simply dissolving them in biocompatible surfactants. One of the dyes identified in the screen was further investigated for NIR-II imaging in mice.

Results and discussion

NIR-II dye screening

13 dyes with absorption in the NIR-II range were obtained from commercial vendors. The structures for 9 of the dyes were provided and are shown in Fig. S1 of the ESI.† To rapidly screen the dyes, small amounts of the powders were added to water to form a uniform insoluble suspension, from which a volume was withdrawn and dissolved into various solubilization systems. The dye suspensions were dissolved in Kolliphor HS 15 (HS15), Tween 80, Cremaphor EL, or cyclodextrins solutions at a final concentration of 10% (w/w or w/v). Propylene glycol included ethanol and water at a volume ratio of 40 : 10 : 50. Methanol and phosphate buffered saline (PBS) were control solvents. Samples were sonicated and centrifuged to remove particulate matter, and the absorption of the supernatant at 1064 nm was assessed, since this is the output wavelength of the Nd:YAG laser commonly used for PAI. As shown in Fig. 1A, dissolving the dyes in the methanol generally

induced the highest calculated absorption (*i.e.* observed absorbance multiplied by the dilution factor). The maximum absorption wavelength for the dyes in the surfactants was generally between 1000–1100 nm (Table 1). Absorption at the maximum wavelength are shown in Fig. S2 of the ESI.†

The screen revealed the dyes S01452, S01968 and benzo indole butyl diphenylaminocyclopentene heptamethine tetrafluoroborate (BIBDAH) as candidates for further evaluation (Fig. 1B). These had similarities in their structures, including being symmetric heptamethine cyanines with benzoindole groups in the form of tetrafluoroborate salts. The dye counter ion appeared significant, since when BIBDAH had tetrafluoroborate replaced with a bis trifluoromethane sulfonyl imide counterion (S08734), solubilization efficacy decreased.

The screen did not involve an initial dissolution step in organic solvent, since the goal was to assess the simplest dye formulation method. Doing so might yield different results. Many of the dyes assessed did not dissolve in methanol, so

Table 1 Maximum absorption wavelength of dyes (1 mg mL^{-1}) in indicated surfactants (10%). Asterisk indicates a weak resulting absorption intensity value of less than 1

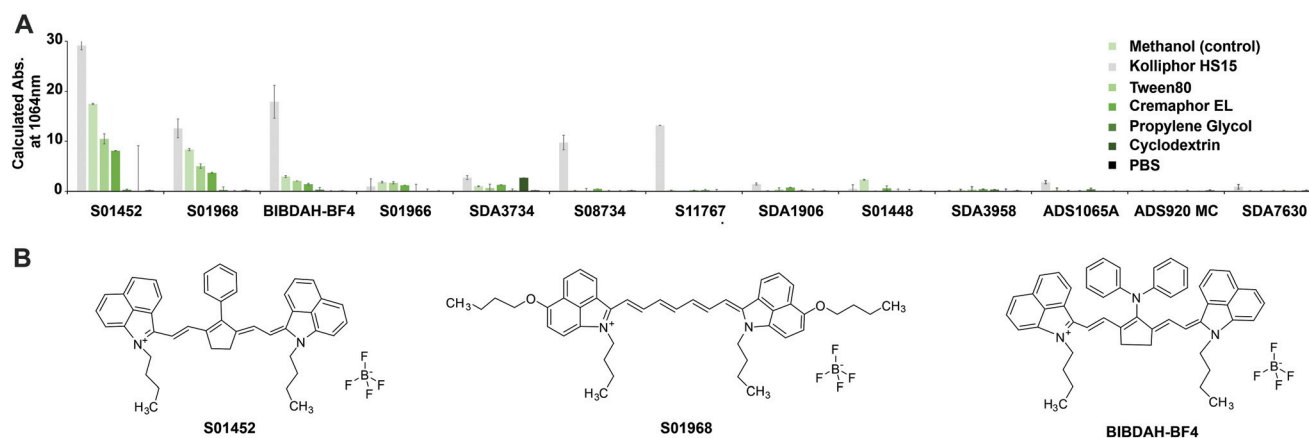| Dye	Tween 80	Cremaphor EL	Kolliphor HS15
ADS920MC	1036*	1068*	1054*
ADS1065A	1064*	1100*	934*
S01448	1080*	1082*	1082
BIBDAH	1028	1030	1030
S01452	1052	1058	1054
S01966	992	1020	988
S01968	1028	886	902
S11767	1030*	1058*	1056*
SDA1906	1030*	1058*	1098*
SDA3734	1024*	1058	1012
SDA3958	964	986	966
SDA7630	1026*	1058*	1098*
S08734	1028*	1020	1098*

Fig. 1 Screening NIR-II dyes with simple formulation in solubilization systems suitable for intravenous delivery. (A) Calculated absorption at 1064 nm of indicated dyes after formulation in the indicated solvent or surfactant systems. The final concentration of the indicated solubilization agent was 10% (v/v or v/w) in phosphate buffered saline (PBS), with the exception of propylene glycol, which had a final concentration was 40% with 10% ethanol. Methanol is a control solvent that is not a suitable carrier for intravenous administration. Error bars show std. dev., *n* = 3. (B) Chemical structures of the indicated dyes.

less polar solvents like dichloromethane would be required. Indeed, S08734 showed little NIR-II absorption in this screen, but previously generated intensely absorbing NIR-II micelles when first dissolved in dichloromethane prior to mixing in surfactant.[27] For the dyes that could be solubilized, cyclodextrin and propylene glycol were ineffective. Tween 80, HS15 and Cremaphor EL provided solubilization, although the resulting absorption was diminished relative to methanol, implying that conditions could be improved for better dissolving the dye.

Formulation optimization

BIBDAH, S01452 and S01968 were further assessed to determine how the type and concentration of dye and surfactant related to the resulting NIR-II absorption. Dyes were dissolved in 10% surfactant at varying concentrations from 0.5 to 5 mg mL^{-1} and sonicated at 60 °C. In these conditions, the dyes reached an absorbance plateau at the concentration range of 1–3 mg mL^{-1} of dye (Fig. 2A–C), implying this was the maximum capacity for surfactant micelles to load the dye. Next, increasing surfactant concentration was assessed. As shown in Fig. 2D–F, a trend was observed for all dyes, showing that higher surfactant concentrations resulted in greater dye

solubilization. Tween 80, Cremophor EL and HS15 all were able to solubilize the dyes effectively, with no major differences were observed between them. Of the three dyes, BIBDAH generally produced the highest absorption values at 1064 nm. Based on initial screening results, HS15 appeared to produce the highest NIR-II absorption values. At 5 mg mL^{-1} dye in 25% surfactant, some insoluble material was observed when the sample was centrifuged. This could be eliminated by reducing the concentration to 1 mg mL^{-1}.

1 mg mL^{-1} of dyes were dissolved in 25% HS15 in PBS, sonicated, and sterile filtered through a 0.2 μm membrane. The initial calculated absorption of the formulations is shown in Fig. 3A. A shoulder peak around 900 nm was observed in all dyes, but was substantially greater in S01452 and S01968 formulations, where prominent second peaks formed. BIBDAH had just a single absorption maximum at 1030 nm with substantially greater magnitude. The secondary peaks can likely be attributed to the dye in an aggregated form. Thus, the singular peak of the BIBDAH formulation implies the dye was better solubilized in the HS15 micelles compared to the other two.

The stability of the formulations in refrigerated storage was assessed over 6 weeks (Fig. 3B). The absorption of S01452 decreased to less than half of its initial value in the first week before stabilizing somewhat. BIBDAH and S01968 were more stable in storage, although a modest decrease of approximately 20% occurred over 6 weeks, based on the NIR-II absorption. Throughout this period, BIBDAH retained a calculated absorbance maximum of over 100.

The behavior of sterile-filtered BIBDAH (1 mg mL^{-1}) in PBS with HS15 (25%) was evaluated following intravenous injection to mice (10 mg kg^{-1}). The absorption of sampled blood plasma was measured. Strong NIR-II absorption, with minimal background, was apparent in collected plasma, with a singular peak at 1034 nm (Fig. 4A). NIR-II absorption of circulating plasma decreased over time, but remained clearly detectable until at least 6 hours. The half-life of the BIBDAH in 25% HS15 in blood was 1.07 h (Fig. 4B).

Like most cyanine dyes, BIBDAH exhibited fluorescence emission, with a peak emission wavelength close to 1070 nm when excited with a 980 nm light source. A long emission tail produced substantial signal up to 1300 nm, so that a 1200 nm
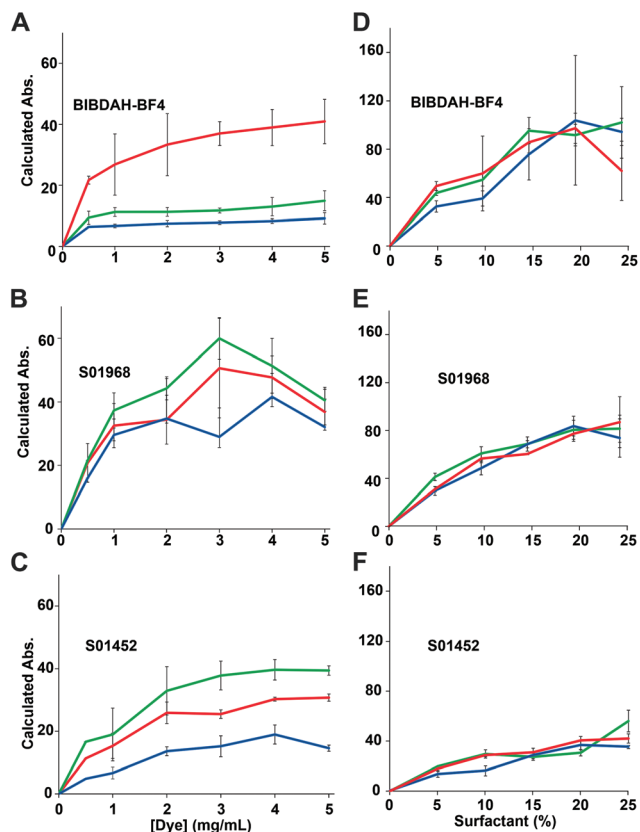

Fig. 2 Varying solubilization conditions for NIR-II dyes. Dyes were dissolved in indicated conditions, sonicated, and centrifuged to remove insoluble materials and absorption at 1064 nm was assessed at varying dye concentrations in 10% surfactant (A–C) and at varying surfactant concentrations at 5 mg mL^{-1} dye (D–F). Error bars: std. dev., n = 3. Lines indicate Kolliphor HS15 (red), Tween 80 (green), or Cremaphor EL (blue).
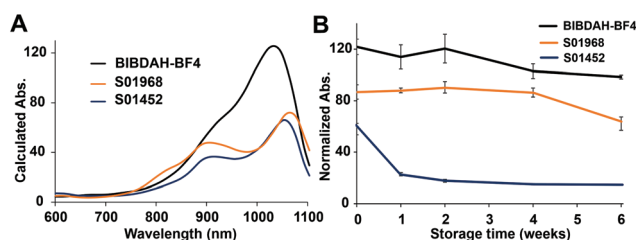

Fig. 3 Absorption spectra and storage stability of dye formulations. (A) Absorbance spectra of a formulation of 1 mg mL^{-1} dye in PBS with 25% HS15. (B) Storage stability of the formulations at 4 °C, as measured by absorbance. Error bars: std. dev. of mean, n = 5 dye preparations.
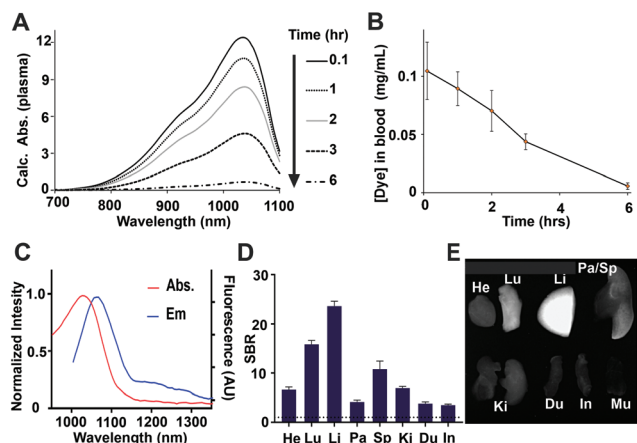
Fig. 4 Intravenous administration of BIBDAH in HS15 to mice (10 mg kg^{-1}). (A) Plasma absorption following injection. Plasma was diluted up to 20 fold for measurement. (B) Pharmacokinetic profile of BIBDAH in blood. (C) Fluorescence emission of BIBDAH in PBS. (D) Fluorescent signal to background ratio (SBR; relative to muscle) biodistribution of BIBDAH, 4 h post-injection (E) fluorescence image of dissected heart (He), lungs (Lu), liver (Li), pancreas (Pa), spleen (Sp), kidneys (Ki), duodenum (Du), intestine (In) and muscle (Mu) Error bars: std. dev, $n = 3$ mice per group.

Fig. 5 Photoacoustic imaging in phantoms and *in vivo* with BIBDAH. (A) Plot of PA signal at varying concentration of BIBDAH. (B) Phantom imaging in milk; signal evaluated by depth. (C) *In vivo* imaging of nude mice bearing MIA PaCa-2 tumors prior to and 6 h after intravenous injection of 10 mg kg^{-1} BIBDAH. The tumor region is indicated by a white square. Error bars: standard deviation, $n = 3$.

long pass filter could be used for fluorescence imaging, which is an approach used for other NIR-II dyes to minimize interference of autofluorescence from the body.[28–31] 4 h after administration, once most of the dye had left the blood, imaging was used to assess organ biodistribution (Fig. 4D and E). From the imaging data, it is apparent that most of the dye was uptaken in the liver, with some uptake also observed in the lungs and spleen. Based on the strong liver uptake, taken together with the lack of dye signal observed in the kidneys,
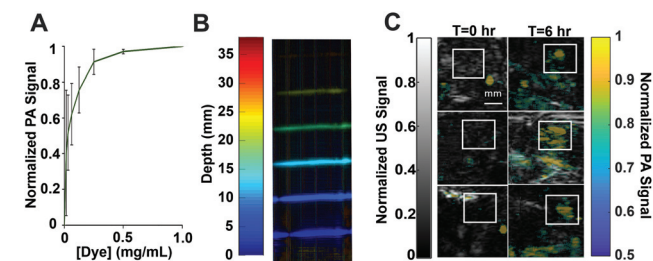
minimal renal clearance was observed for this BIBDAH formulation. Prior studies have shown that NIR-II probes can be developed with effective renal clearance.[18,32] A contrast agent that clears from the body through renal filtration generally does so more quickly and effectively than other elimination routes and has safety advantages. Further studies would need to identify whether BIBDAH binds to blood components that lead to rapid liver uptake or if alternate formulations could encourage renal filtration.

Next, BIBDAH was assessed for suitability as a photoacoustic contrast agent. The dye was evaluated in phantoms at different diluted concentrations (Fig. 5A). Photoacoustic signal increased with increasing dye concentration, as expected. Fig. 5B shows a varying-depth phantom submersed in 1:8 whole milk to water ratio to mimic the tissue scattering.[33] The BIBDAH concentration was kept constant at 0.5 mg mL^{-1}. The dye could be observed at 2.5 cm depth in the tissue-mimicking phantom.
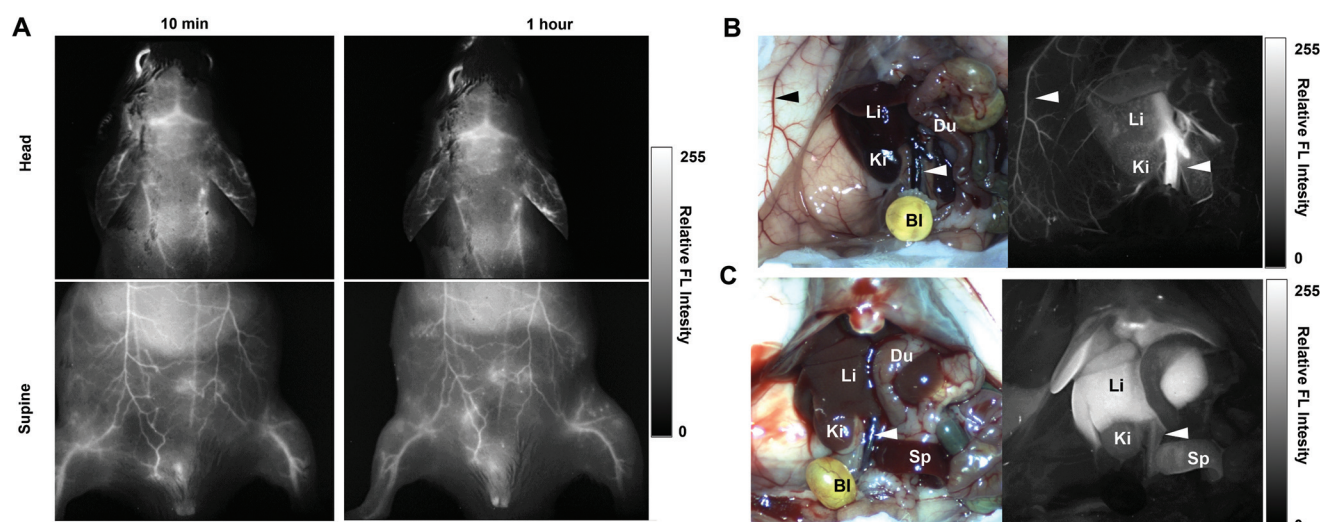

Fig. 6 Fluorescence NIR-II imaging using BIBDAH: (A) Fluorescence images of mouse head and abdomen following intravenous injection of 0.1 mg BIBDAH per mouse and excitation with a 980 nm laser. Images were collected using a 1200 nm long pass filter at 10 min and 1 hour post injection. (B) White light and fluorescence images of abdomen after opening at 30 min (B) and at 4 h (C) post injection. Arrows show the inferior vena cava and an epigastric vein. Representative images from $n = 3$ mice.

To assess whether the dye could be useful for photoacoustic imaging in animals, nude mice bearing human MIA PaCa-2 pancreatic subcutaneous tumors were intravenously administered with the BIBDAH formulation. Tumors were imaged prior to injection and 6 h afterwards. As shown in Fig. 5C, in all three tumor-bearing mice, clear uptake in the tumor region (denoted by the white boxes) was observed, compared to the same regions prior to dye administration.

The dye was next assessed for fluorescence imaging in mice. Fig. 6A shows that at 10 minutes and also 1 h after intravenous injection, strong fluorescence signal could be observed through the skin, in the underlying blood vessels. Intensity profiles across blood vessels in the supine position are shown in Fig. S3 of the ESI.† The distinguishable surface blood vessels generally had 25–50% greater signal than the background signal from the adjacent abdomen skin. Under these imaging conditions, minimal autofluorescence is present, so the background originated from scattering of the dye signal in smaller or deeper blood vessels. Brain vessels were observed through the intact skull. In mice with the abdomen cavity opened, the dye could initially be observed confined in major blood vessels in the liver and elsewhere. Over the next few hours, as the dye was cleared from the circulatory system (Fig. 4B), BIBDAH could be observed directly migrating to the liver in mice.

Conclusions

We identified the dye BIBDAH by screening commercially-available NIR-II dyes for those that could be easily dissolved in biocompatible surfactants. The HS15-based formulation developed here can be readily prepared for administration to animals without the requirement of specialized equipment or need for purification. BIBDAH in HS15 has favorable properties in terms of NIR-II absorption, fluorescence, and storage stability. NIR-II imaging of tumor tissues and blood vessels was straightforward using this approach. This study did not address potential toxicity concerns of BIBDAH nor its BF4 counter-ion, and this should be done in the future.

Experimental

Materials

ADS920MC and ADS1065A dyes were purchased from American Dye Source; SDA1906, SDA3734, SDA3958 and SDA7630 were purchased from H. W. Sands Corp, and S01448, BIBDAH-BF4 (S01451), S01452, S01966, S01968, S08734 and S11767 were purchased from Spectrum Dyes & Chemicals. Cremaphor EL (#C5135), Kolliphor HS15 (#42966), Tween 80 (#P1754), and Propylene Glycol (#W294004) were purchased from Sigma-Aldrich. Cyclodextrin-β (#RC-0C7-020) was purchased from Captisol.

Screening dyes for simple solubilization

Stock solutions were made of 2 mg mL^{-1} for all dyes in PBS as insoluble suspensions. Cremaphor EL (viscous liquid), Kolliphor HS15 (paste), Tween 80 (viscous liquid), and cyclodextrin (powder) were made as 20% (w/v or v/v) stock solutions. With a 1 : 1 dilution of the dye suspension and surfactant, the final dye concentration was 1 mg mL^{-1} of dye with 10% surfactant in 137 mM NaCl pH 7.4 PBS. For propylene glycol and ethanol, a 2× solution was prepared so that after dilution, the final ratio was 40 : 10 : 50 propylene glycol : ethanol : water with 1 mg mL^{-1} of dye. For methanol and acetone 40 : 160 μL, dye to solvent ratio was used and the absorbance was adjusted by a calculation of 250×. All samples were sonicated at 60 °C for 30 min, then centrifuged for 3 min at 1000 rcf. Then the supernatant was measured by spectrophotometer (Lambda 365 UV/Vis by PerkinElmer), 10 μL of surfactant and dye solution were diluted by 990 μL of PBS for surfactants otherwise directly in the solvent. A total of 1000 μL in a cuvette with a 1 cm pathlength. Absorbance values were multiplied by the dilution factor (100) to find the maximum calculated absorbance as well as the calculated absorbance at 1064 nm.

Varying dye and surfactant concentrations

To assess the dyes at varying dye concentrations, each dye stock solution in PBS was made at 1, 2, 4, 6, 8, 10 mg mL^{-1} and diluted 1 : 1 with 20% surfactants of Tween 80, Kolliphor HS15, and Cremaphor EL for ending concentration of 10% surfactant. Samples were sonicated at 60 °C for 30 min, then centrifuged for 3 min at 1000 rcf. Then the supernatant was measured by spectrophotometer, 10 μL of surfactant and dye solution were diluted by 990 μL of 137 mM NaCl pH 7.4 PBS for solvents or solvent for solvent in a cuvette. Then, absorbances were multiplied by 100× (or 250× for solvents) to get calculated absorbances and from there maximum absorbance. To assess the dyes at varying surfactant concentrations, a dye stock suspension solution in PBS was made at 10 mg mL^{-1} and diluted 1 : 1 with 10, 20, 30, 40, or 50% surfactant of Tween 80, Kolliphor HS15, and Cremaphor EL. The resulting concentration(s) of 5, 10, 15, 20, or 25 (%) surfactant, and 5 mg mL^{-1} for dye. All samples were sonicated at 60 °C for 30 min, then centrifuged for 1 min at 1000 rcf. The supernatant was then measured by spectrometer, 10 μL of surfactant and dye solution were diluted by 990 μL of PBS in a cuvette. Absorbance values were multiplied by the dilution factor (100) to find the maximum calculated absorbance.

Dye preparation for stability and animal studies

Dyes were prepared by dissolving them in 137 mM NaCl pH 7.4 PBS. The final concentration of each dye was 1 mg mL^{-1} and 25% HS15. Samples were sonicated at 60 °C for 30 min and then passed through a 0.2 μm sterile filter membrane from Thomas Scientific, Catalog #1190M42. After preparation samples were stored refrigerated at 4 °C and periodically sampled. For each time point, 10 μL of dye was diluted into

990 μL of PBS for reading in spectrometer. The point chosen for comparison with the standard curve was 1064 nm.

Pharmacokinetics

Pharmacokinetic studies were performed in compliance with protocols approved by the University at Buffalo IACUC. 8-week old female ICR mice from Charles River Laboratories were used., 200 μL of dye (0.2 mg) was injected into the tail vein of the mouse for a 10 mg kg^{-1} dose. Blood was sampled at 0.1, 1, 2, 3, and 6 h time points. For initial time points, 20 μL of blood was gathered with capillary blood collection tubes with EDTA powder from Thermo Fisher Scientific (#NC9059691). At the 3 and 6 h time points, 30 μL and 50 μL was taken, respectively. Blood samples are centrifuged at 3000 rcf for 10 min to separate plasma from whole blood. If 20 μL, 30 μL or 50 μL was collected 10 μL, 20 μL and 30 μL of plasma was diluted respectively in PBS, 190 μL, 180 μL, and 170 μL for a 20×, 10× and 6.67× solution that was read by the spectrophotometer. The spectral values were multiplied by the dilution factor to plot the calculated absorption.

Photoacoustic imaging *in vitro*

For all experiments, the photoacoustic excitation source was a 10 ns, 10 Hz pulse repetition rate Nd:YAG laser (Continuum SL III) with output wavelength of 1064 nm. A linear array transducer (Imasonic SAS) with central frequency of 2.25 MHz is used as the PAI detector. The PAI data was acquired using a 256-channel data acquisition system (Verasonics, Inc.). For phantom experiments, a 3D model was made in Solidworks, and holes were made for 2 mm tubing with 1 mm diameter, spaced 5 mm apart and printed on a 3D printer (Uprint by Stratasys), similar to a previously reported approach.[34] Next, dye was added to each tube at different dilutions. The tubes were closed off by knotting the ends then immersed in water and scanned in sequence using the linear transducer array. The energy of the laser is measured as 75 mJ per pulse. The signal-to-noise ratio is determined and plotted against dye concentration as shown in Fig. 5A. In order to determine PAI depth of the dye in tissue mimicking scattering medium, we designed another study where the tubes are placed at different depths immersed in 1 : 7 milk to water mixture.[33] The tubes were scanned with the same linear transducer array. The depth-encoded maximum intensity projection (MIP) of the reconstructed PA image is shown in Fig. 5B.

In vivo photoacoustic imaging

Nude, female, 8-week old mice from Charles River Laboratories with ~1 cm MIA PaCa tumors were used. IV injection of 200 μL with 25% Kolliphor HS15 and 1 mg mL^{-1} BIBDAH-BF4 was administrated through the tail vein. Each mouse was initially anesthetized with 3% Isoflurane inhalation, and was then maintained under 0.5–1% Isoflurane concentration during imaging. The mice were also placed on a heat pad to maintain body temperature while under anesthesia. The imaging platform contains a water tank with an imaging window at the bottom, sealed by a thin plastic mem-

brane. The mouse was placed beneath the plastic membrane with ultrasound gel (Parker Laboratories, Inc.) applied to the tumor for acoustic coupling. Each mouse was scanned pre-injection and 6 hours post injection using a Philips L7-4 linear array transducer with 128 elements and 5 MHz central frequency. Both PAI and ultrasound data are acquired simultaneously. Normalized PAI data overlaid on ultrasound is shown in Fig. 5C. For all animal experiments, the laser intensity on animal surface was around 7.2 mJ cm^{-2}, which was well below the ANSI safety limit of 100 mJ cm^{-2} for 1064 nm light.[32]

Fluorescence imaging in the NIR-II region

Animals were housed in an AAALAC-certified facility and were studied under the protocols approved by the MGH IACUC. Six-week-old CD-1 mice (male; 25–30 g) were purchased from Charles River Laboratories (Wilmington, MA, USA). Mice were maintained under anesthesia with isoflurane and oxygen during the experiment. Before injection, mice's fur was removed. A 100 μL of 25% Kolliphor HS15 in PBS (pH 7.4, 1 mg mL^{-1}) was injected through the tail vein. Mice were imaged with skin intact using a 640 × 512-pixel InGaAs camera (Ninox640, Raptor Photonics) with customized software. A 980 nm fiber coupled diode laser (20 mW cm^{-1}) was used as an excitation source, and 1200 nm long-pass filter (Thorlabs) was used to collect the NIR-II signal. After 4 h post-injection, mice were sacrificed to image organs. At least 3 mice were analyzed for each sample.

Conflicts of interest

There are no conflicts to declare.

Acknowledgements

References

1 E. M. Sevick-Muraca, *Annu. Rev. Med.*, 2012, **63**, 217–231.
2 R. M. Schols, N. J. Connell and L. P. S. Stassen, *World J. Surg.*, 2015, **39**, 1069–1079.
3 M. Xu and L. V. Wang, *Rev. Sci. Instrum.*, 2006, **77**, 041101.
4 C. Li, Y. Zhang, M. Wang, Y. Zhang, G. Chen, L. Li, D. Wu and Q. Wang, *Biomaterials*, 2014, **35**, 393–400.
5 G. Hong, J. T. Robinson, Y. Zhang, S. Diao, A. L. Antaris, Q. Wang and H. Dai, *Angew. Chem., Int. Ed.*, 2012, **51**, 9818–9821.
6 B. Dong, C. Li, G. Chen, Y. Zhang, Y. Zhang, M. Deng and Q. Wang, *Chem. Mater.*, 2013, **25**, 2503–2509.

7 C.-N. Zhu, P. Jiang, Z.-L. Zhang, D.-L. Zhu, Z.-Q. Tian and D.-W. Pang, *ACS Appl. Mater. Interfaces*, 2013, **5**, 1186–1189.

8 Y. Nakane, Y. Tsukasaki, T. Sakata, H. Yasuda and T. Jin, *Chem. Commun.*, 2013, **49**, 7584–7586.

9 Y. Zhang, Y. Zhang, G. Hong, W. He, K. Zhou, K. Yang, F. Li, G. Chen, Z. Liu, H. Dai and Q. Wang, *Biomaterials*, 2013, **34**, 3639–3646.

10 Q. Miao and K. Pu, *Adv. Mater.*, 2018, **30**, 1801778.

11 Y. Jiang, P. K. Upputuri, C. Xie, Y. Lyu, L. Zhang, Q. Xiong, M. Pramanik and K. Pu, *Nano Lett.*, 2017, **17**, 4964–4969.

12 K. Shou, Y. Tang, H. Chen, S. Chen, L. Zhang, A. Zhang, Q. Fan, A. Yu and Z. Cheng, *Chem. Sci.*, 2018, **9**, 3105–3110.

13 Y. Fan, P. Wang, Y. Lu, R. Wang, L. Zhou, X. Zheng, X. Li, J. A. Piper and F. Zhang, *Nat. Nanotechnol.*, 2018, **13**, 941–946.

14 Y.-S. Chen, Y. Zhao, S. J. Yoon, S. S. Gambhir and S. Emelianov, *Nat. Nanotechnol.*, 2019, **14**, 465–472.

15 J.-E. Park, M. Kim, J.-H. Hwang and J.-M. Nam, *Small Methods*, 2017, **1**, 1600032.

16 P. Vijayaraghavan, C.-H. Liu, R. Vankayala, C.-S. Chiang and K. C. Hwang, *Adv. Mater.*, 2014, **26**, 6689–6695.

17 Y. Sun, C. Qu, H. Chen, M. He, C. Tang, K. Shou, S. Hong, M. Yang, Y. Jiang, B. Ding, Y. Xiao, L. Xing, X. Hong and Z. Cheng, *Chem. Sci.*, 2016, **7**, 6203–6207.

18 A. L. Antaris, H. Chen, K. Cheng, Y. Sun, G. Hong, C. Qu, S. Diao, Z. Deng, X. Hu, B. Zhang, X. Zhang, O. K. Yaghi, Z. R. Alamparambil, X. Hong, Z. Cheng and H. Dai, *Nat. Mater.*, 2016, **15**, 235–242.

19 S. Wang, Y. Fan, D. Li, C. Sun, Z. Lei, L. Lu, T. Wang and F. Zhang, *Nat. Commun.*, 2019, **10**, 1058.

20 C. Sun, B. Li, M. Zhao, S. Wang, Z. Lei, L. Lu, H. Zhang, L. Feng, C. Dou, D. Yin, H. Xu, Y. Cheng and F. Zhang, *J. Am. Chem. Soc.*, 2019, **141**, 19221–19225.

21 Y. Zhou, D. Wang, Y. Zhang, U. Chitgupi, J. Geng, Y. Wang, Y. Zhang, T. R. Cook, J. Xia and J. F. Lovell, *Theranostics*, 2016, **6**, 688–697.

22 S. Zhu, R. Tian, A. L. Antaris, X. Chen and H. Dai, *Adv. Mater.*, 2019, **31**, 1900321.

23 J. Huang, Y. Jiang, J. Li, S. He, J. Huang and K. Pu, *Angew. Chem., Int. Ed.*, 2020, **59**, 4415.

24 R. Tian, Q. Zeng, S. Zhu, J. Lau, S. Chandra, R. Ertsey, K. S. Hettie, T. Teraphongphom, Z. Hu, G. Niu, D. O. Kiesewetter, H. Sun, X. Zhang, A. L. Antaris, B. R. Brooks and X. Chen, *Sci. Adv.*, 2019, **5**, eaaw0672.

25 S. Gao, G. Wei, S. Zhang, B. Zheng, J. Xu, G. Chen, M. Li, S. Song, W. Fu, Z. Xiao and W. Lu, *Nat. Commun.*, 2019, **10**, 2206.

26 Y. Zhang, M. Jeon, L. J. Rich, H. Hong, J. Geng, Y. Zhang, S. Shi, T. E. Barnhart, P. Alexandridis, J. D. Huizinga, M. Seshadri, W. Cai, C. Kim and J. F. Lovell, *Nat. Nanotechnol.*, 2014, **9**, 631–638.

27 U. Chitgupi, N. Nyayapathi, J. Kim, D. Wang, B. Sun, C. Li, K. Carter, W.-C. Huang, C. Kim, J. Xia and J. F. Lovell, *Adv. Mater.*, 2019, **31**, 1902279.

28 S. Zhu, R. Tian, A. L. Antaris, X. Chen and H. Dai, *Adv. Mater.*, 2019, e1900321, DOI: 10.1002/adma.201900321.

29 Y. Zhong, Z. Ma, F. Wang, X. Wang, Y. Yang, Y. Liu, X. Zhao, J. Li, H. Du, M. Zhang, Q. Cui, S. Zhu, Q. Sun, H. Wan, Y. Tian, Q. Liu, W. Wang, K. C. Garcia and H. Dai, *Nat. Biotechnol.*, 2019, **37**, 1322–1331.

30 Y. Fan, P. Wang, Y. Lu, R. Wang, L. Zhou, X. Zheng, X. Li, J. A. Piper and F. Zhang, *Nat. Nanotechnol.*, 2018, **13**, 941–946.

31 H. Kang, W. R. Stiles, Y. Baek, S. Nomura, K. Bao, S. Hu, G. K. Park, M. J. Jo, H. I, J.-L. Coll, B. P. Rubin and H. S. Choi, *Adv. Mater.*, 2020, **32**, 1905899.

32 J. Huang, C. Xie, X. Zhang, Y. Jiang, J. Li, Q. Fan and K. Pu, *Angew. Chem., Int. Ed.*, 2019, **58**, 15120–15127.

33 G. Mitic, J. Kolzer, J. Otto, E. Plies, G. Solkner and W. Zinth, *Appl. Opt.*, 1994, **33**, 6699–6710.

34 S. J. Arconada-Alvarez, J. E. Lemaster, J. Wang and J. V. Jokerst, *Photoacoustics*, 2017, **5**, 17–24.